Submicrometer Cavity Surface Plasmon Sensors

Dragos Amarie,[†,‡] Tiberiu-Dan Onuta,[†,‡] Radislav A. Potyrailo,[§] and Bogdan Dragnea*[,†]

Departments of Chemistry and Physics, Indiana University, Bloomington, Indiana 47405, and GE Global Research Center, Niskayuna, New York 12309

Received: May 13, 2005; In Final Form: June 21, 2005

A miniaturized spherical surface plasmon sensor for measuring the binding kinetics of unlabeled molecules is introduced. The sensor has a submicrometer footprint with a sensitivity that rivals that of state-of-the-art commercial planar surface plasmon sensors, which makes it valuable for applications requiring integration of detection of molecular species in microfluidic channels. The basic principle of the sensor is exploiting the wavelength shifts of the cavity resonances of a metal-coated submicrometer sphere embedded in an opaque metal film due to molecular adsorption. The sensor has been found to be exquisitely responsive in air to water and ethanol vapor adsorption on the bare gold sensor surface. When immersed in a liquid, the sensor can detect the adsorption of less than one monolayer of dodecanethiol (∼1.5 nm) on the gold coating of the sphere.

Introduction

Surface plasmon (SP) polariton resonances are a well-known phenomenon which has enabled the development of a series of powerful technologies for superresolution imaging,[1,2] optoelectronics,[3,4] and bioanalysis.[5−7] For biomolecular interaction analysis, the principal advantages of the SP resonance techniques are nonintrusiveness, real-time binding monitoring, and label-free conditions.[8]

With the advent of microfluidic devices, the trend in analytical systems is to scale down many of the existing bioanalytical technologies with the main goal of achieving increasingly parallel throughput while decreasing the required sample amount. Despite these unique features, SP sensor integration in microfluidic channels at a submicrometer scale has not been achieved until now. Conventional, planar sensors require, for efficient conversion of light into SPs, strict angles of incidence of the light on the active surface as well as polarization orientation. Therefore, one difficulty to overcome in miniaturizing the sensor comes from the fact that, as the active sensor surface shrinks, the sensitivity is affected because of the wider angular distribution resulting from focusing and the simultaneous decrease in the total number of binding sites within the spot.

Therefore, adding a mechanism to increase the sensitivity is necessary to alleviate these challenges. One possible solution is replacing the propagating plasmon wave with a stationary one or, in other words, enhancing the sensitivity by adding a shape resonance. Such a stationary wave will travel across the active surface a number of times proportional to the quality factor of the resonance, thus increasing the probability of interaction between the wave and the adsorbate, similar to a multipass cell for spectroscopy.

The circulation of light within highly symmetric microscopic structures often involves such shape resonances. For dielectric spheres 10−100 μm in size, a particular class of resonances, known as whispering gallery modes, occurs. The name stems from similarities with the phenomenon of circumferential guiding of faint sounds along the walls of the St. Paul's Cathedral gallery in London.[9] Bioanalytical and spectroscopic applications taking advantage of the characteristic of strong surface localization and high quality factors[10] of whispering gallery modes in dielectric microspheres and liquid droplets have already started to emerge.[11−13] However, the whispering gallery modes gradually lose their surface localization properties when the microsphere size is decreased. For submicrometer sizes, one way to maintain light confinement is to coat the sphere with an SP-supporting metal film. An interesting characteristic of such a microsphere coated with a metal film is expected to occur: at certain diameters, the total internal reflection angles associated with cavity modes may coincide with an SP resonance angle for the metal film, thus resulting in an efficient form of SP excitation on spherical surfaces. In other words, the stringent geometric conditions from planar sensors are relaxed. In the present paper we discuss the occurrence, the features, and the possibilities of use of such resonances for miniaturized surface plasmon sensors.

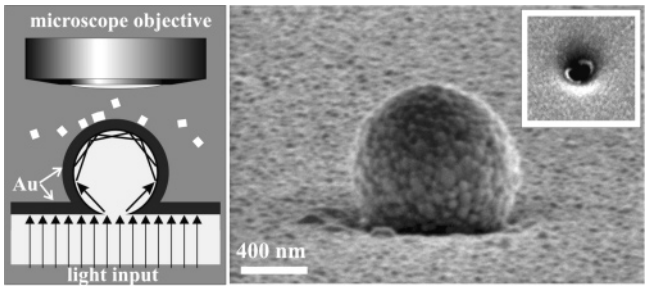

Figure 1. Schematic of the resonant microcavity surface plasmon sensor and a scanning electron micrograph of its experimental realization. Dielectric sphere diameter 770 nm. Inset: a 500 nm × 500 nm micrograph of a typical subwavelength pinhole remaining in the metal film after the bead removal. The metal film (thickness ∼150 nm) has been ion-sputtered on the glass support.

Experimental Section

Figure 1 shows a schematic and a scanning electron micrograph of the submicrometer spherical cavity sensor. The samples

* To whom correspondence should be addressed. E-mail:dragnea@indiana.edu.
† Department of Chemistry, Indiana University.
‡ Department of Physics, Indiana University.
§ GE Global Research Center.

10.1021/jp052536i CCC: $30.25
Published on Web 07/22/2005

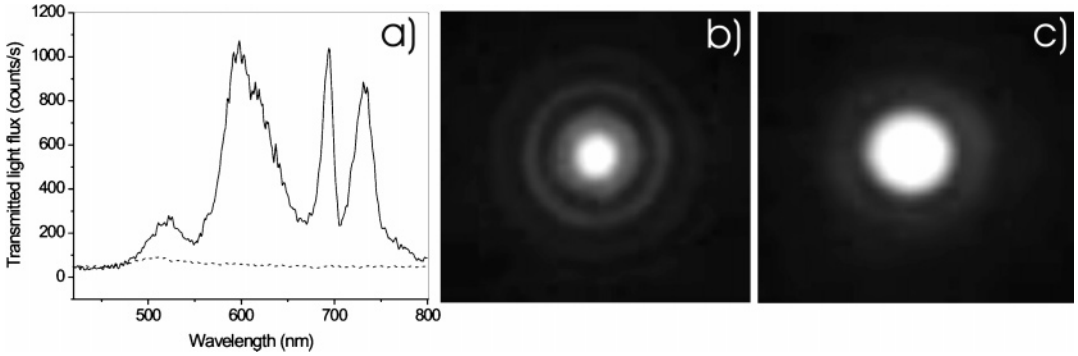

Figure 2. (a) Continuous line: spectrum of the light emitted from a Au-coated bead imbedded in a Au film and illuminated from the other side by white light (raw counts, 400−800 nm) from a microscope illuminator. Dashed line: spectral transmission of the compact Au film. The ∼60 cps background corresponds to the dark current of the photodetector. (b) Normalized, 3.3 μm × 3.3 μm CCD image of the pattern of light intensity emerging from a Au-coated bead. (c) Normalized light intensity pattern emerging from a cylindrical hole obtained by nanosphere lithography of an evaporatively coated film.[14] Everywhere in the figure the bead diameter is 770 nm and the Au coating thickness is 150 nm.

are obtained by spreading a solution of dielectric spheres onto a clean glass substrate followed by vacuum-drying and argon atmosphere sputter coating with a metal (Au, Pt, Pd) of both the bead and the substrate. The sputtering procedure ensures that the bead is uniformly covered with metal. After bead removal, SEM micrographs clearly show the existence of a metal layer even deep inside the cusp formed between the bead and the flat support, Figure 1 (inset). However, a narrow opening (150−200 nm diameter) is left where the dielectric bead contacts the transparent glass support. This near-field aperture is used for direct light coupling into the spherical cavity by using a common microscope Kohler illuminator, Figure 1.

A Nikon TE300 Eclipse inverted microscope, equipped with an oil immersion objective (NA 1.4, 60×, Nikon CFI) and an air objective (NA 0.75, 40×, Nikon CFI), a piezo stage (Polytec PI 500 series), and a monochrome CCD camera (Pixera, EP150), has been used for imaging and single bead selection. Spectra of light scattered from individual coated beads have been acquired using a 300 mm imaging monochromator (Acton Research) equipped with a single-photon-counting avalanche photodiode module (EG&G SPCM) having a dark count rate of 60 cps.

A microscopy cell for liquid handling has been built by lithographic molding of a poly(dimethylsiloxane) (PDMS) chip (∼1 cm thick). Smooth liquid flow through the cell at typical rates of 1 μL/s has been achieved by hydrostatic pressure. Vapor delivery to the sample has been done by allowing access of saturated vapors of water and ethanol to the sample surface. Since the sample and the vapor outlet were enclosed in a tight space, the estimated partial pressures attained were close to 75−80%.

Results and Discussion

A striking optical characteristic of the Au-coated beads is that white-light illumination from the glass side results in a visibly enhanced light transmission with respect to the surrounding planar film at the bead locations, Figure 2b. The spectrum of the transmitted light from a single Au-coated bead is plotted in Figure 2a together with the transmitted light from an area of the film without beads. The spectral transmission is enhanced at particular wavelengths with peak widths sometimes as narrow as 15 nm. The pattern of the light scattered from a bead and collected by a high-NA objective is different from the pattern of the light scattered from a single cylindrical hole fabricated by nanosphere lithography using the same bead diameter and evaporative coating,[14] Figure 2b,c.

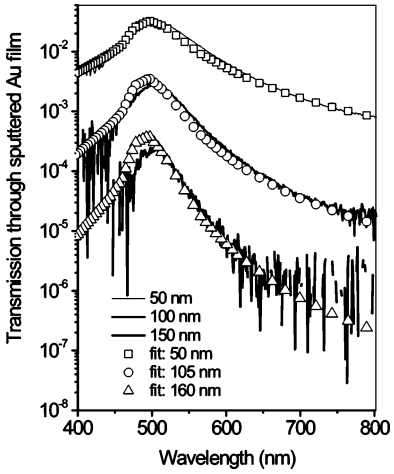

Figure 3. Continuous lines: measured spectral transmission of Au films of different thicknesses, sputter coated on glass. Symbols: calculated transmission using the Au bulk parameters.

We have first investigated the origin of the enhanced light transmission at bead locations. Ar^+ sputter coating is known to provide reasonably even film thickness regardless of the orientation of the surface.[15] It is therefore likely that the bead is uniformly covered and partly embedded in a solid metal film, as confirmed by SEM. However, the film is rough (∼20 nm rms for 150 nm thick films) as can be seen from the SEM image, Figure 1. The film roughness raises the possibility of pinholes. To assess the possible influence of pinholes on the overall transmission, we have compared the simulated spectral transmission of Au films, assumed to have bulk optical properties, with the experimental spectral transmission of sputter coated Au films, Figure 3. The fit is quite good, and thus, at least for films that are thicker than ∼50 nm, the influence of pinholes for direct transmission of light is negligible.

From comparisons of the light transmitted through cylindrical holes and Au-coated single beads, the total transmitted light from a bead corresponds to $\sim 10^{-2}$ from the light that is incident from the other side on the geometrical cross-section of the entire bead. If we take into account that the injection is probably done mostly through the 100−200 nm aperture, which will restrict the amount of light entering the spherical cavity, it follows that we are observing a remarkably strong transmission enhancement with respect to the flat film transmission. Thus, if we consider that the transmission coefficient of the input aperture is somewhere between 1 and 10^{-1} for wavelengths in the visible range, while the film transmission is $\sim 10^{-4}$, a 10^2 to 10^3 transmission coefficient enhancement is observed from the beads

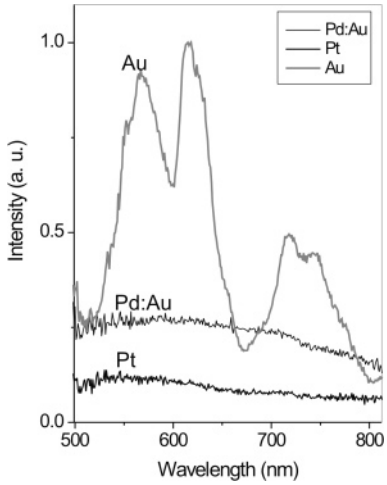

Figure 4. Comparison between the normalized spectra of light scattered from 477 nm diameter beads coated with ~100 nm of Au and similar beads coated with the same thickness of Pd:Au alloy, and Pt.

with respect to a flat film. This enhancement is too strong to be explained by a simple lensing effect coming from the microsphere. In support of this idea, transmission micrographs of 770 nm dielectric beads adsorbed on a glass surface do not exhibit bright spots that are 10^2 to 10^3 times brighter than the background. It is therefore likely that the enhanced transmission occurs through a different mechanism, and the nature of the metal film is likely to play a key role.

To investigate the importance of the nature of the metal film, we have measured the spectrum of light scattered from beads sputter-coated with different metals: Pt, Pd:Au alloy, and Au. The main difference between these metals is that Pd and Pt have strong attenuation coefficients for SP waves with wavelengths in the visible spectrum, while Au has a relatively small attenuation coefficient.[16]

Figure 4 clearly indicates that the observed spectral resonances in the transmitted light occur only for Au-coated beads, and therefore are probably due to an SP-coupling mechanism. Moreover, when inspected under the microscope, the optical contrast in broad-band light between the Au-coated beads and the background from the flat film around them was found to be ~60× larger than the optical contrast observed from Pt- or Pd:Au-coated beads. It is therefore likely that the spectral resonances and the enhanced transmission observed for Au-coated beads are related phenomena and they both depend on the existence of surface plasmon modes.

A significant amount of work has been done on the SP resonances of spherical metal shells with a dielectric core.[17−21] The interest for thin metal shells comes from the fact that SP resonances are different from those of compact metal particles. The dielectric constant and radius of the inner sphere bring two more adjustable parameters, which makes the nanoshell approach promising for a variety of sensing applications.[22] The nanoshell spectral features resulting from the coupling of SPs on the two metal interfaces have been described in terms of hybridization of elementary plasmons supported by nanostructures of elementary geometries (compact metal particles and cavities in bulk metal).[18] The treatment is similar to the one for SPs in thin films where antisymmetric or symmetric couplings can exist between the SPs running on both sides of the film.[16]

The frequency of the symmetric (low-frequency) mode is predicted to increase with the film thickness (blue shift), while the frequency of the high-frequency antisymmetric mode is predicted to decrease with the film thickness (red shift).[16] The splitting into the two hybridized plasmon modes is approximately described by

$$\omega_{l\pm}^{\,2} = \frac{\omega_B^{\,2}}{2}\left[1 \pm \frac{1}{2l+1}\left[1 + 4l(l+1)\left(\frac{a}{b}\right)^{2l+1}\right]^{1/2}\right] \quad (1)$$

where ω_B is the bulk plasma frequency, l is a positive integer equal to the order of spherical harmonics used for decomposition, and a and b are the inner and the outer radii, respectively.[18] The hybridization model has been successfully used to understand the multifeatured plasmon response of thin shells and related aggregates.[18] As a common feature for most of the previous work focusing on plasmon coupling effects, thin films (~10 nm) have been employed. In our case, the maximum contrast between the light scattered from the bead and the light

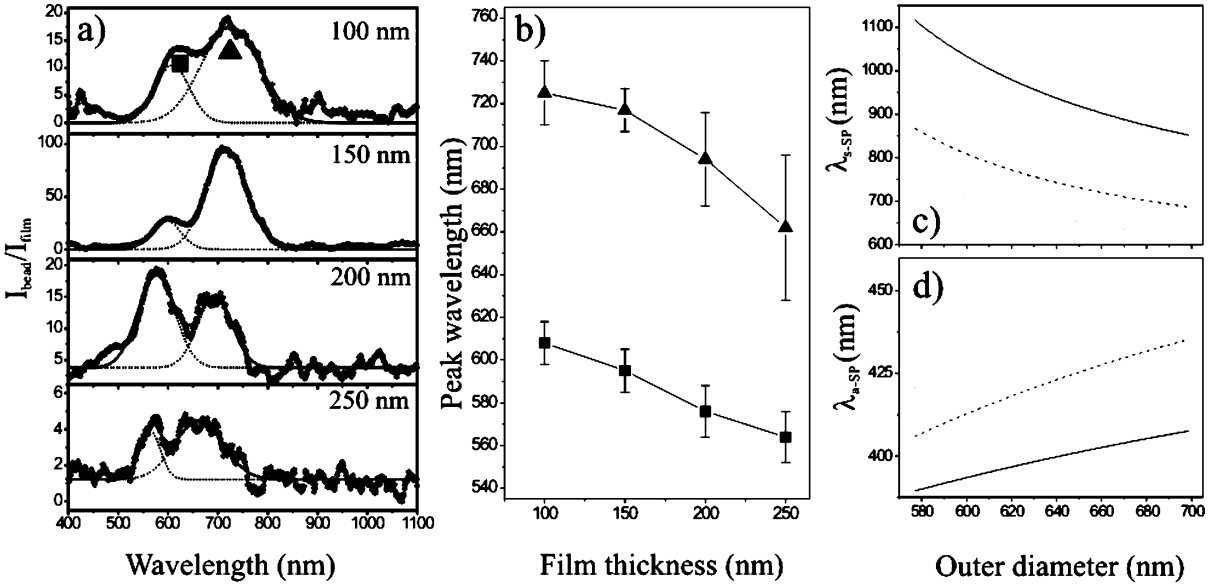

Figure 5. (a) Increasing the film thickness blue shifts the observed resonances of Au-coated 477 nm diameter spheres: dotted line, experimental points; continuous line, multiple peak fitting to obtain the most probable peak position. (b) Peak position as a function of the metal film thickness (see the corresponding symbols in (a)). (c, d) Calculated shift in the antisymmetric (c) and symmetric (d) SP wavelengths as a function of the film thickness for a 477 nm dielectric sphere (dotted line, $l = 3$; dashed line, $l = 2$; continuous line, $l = 1$).

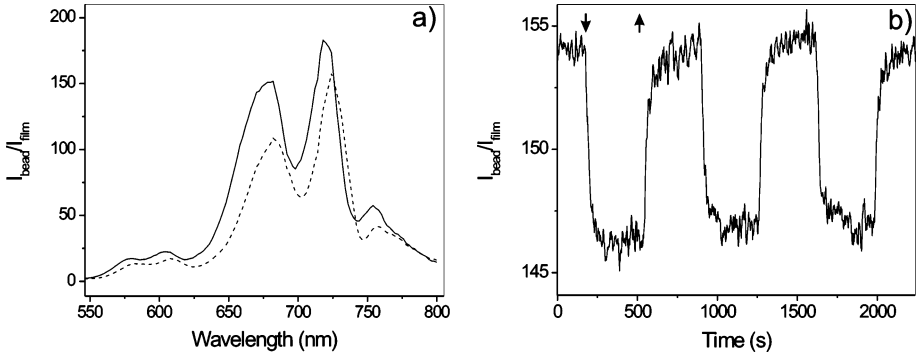

Figure 6. (a) Spectral shifts in the light transmitted from a 770 nm Au-coated bead due to water and ethanol vapor adsorption: continuous line, 50% humidity (ambient atmosphere); dashed line, ~75−80% humidity (vapor access open). (b) Measured sensor response (wavelength 715 nm) to cyclic humidity changes between 50% and 80%. The vertical scale represents the ratio between the maximum intensity of light scattered from the bead and the intensity transmitted by the flat film surrounding it. The arrows represent the instants when the vapor access was open (down) or closed (up).

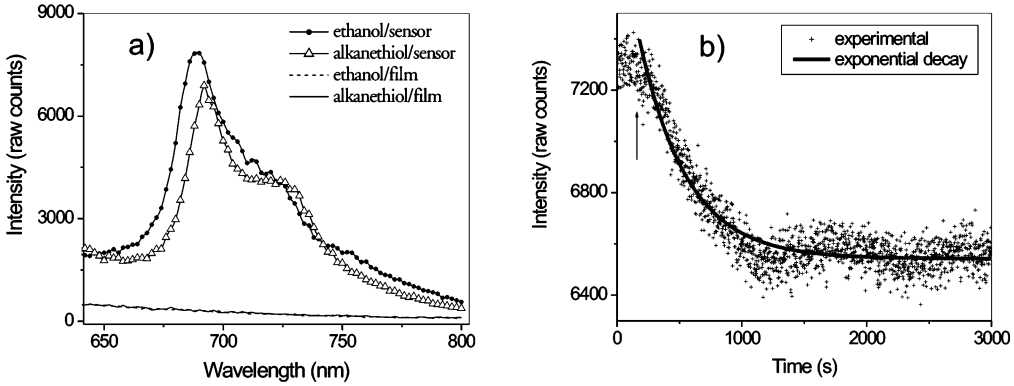

Figure 7. (a) Upon adsorption of a monolayer of dodecanethiol from ethanol, some of the spectral resonances of the light scattered from a Au-coated bead exhibit a red shift. (b) In the case of our polycrystalline Au film, the kinetics of the red shift due to dodecanethiol adsorption can be fitted with a single-exponential decay. The arrow indicates thiol in.

passing through the film is not obtained for thin films, but instead for films thicker than 100 nm, typically.

The question is whether any SP coupling effects can be observed across a 100 nm thick Au film? In the previous experiments done on nanoshells it was essential to use a thin film because the excitation field and the detector are both outside the shell and scattered light is detected. In our case, the excitation field is *inside* the shell and the detection is done *outside*. The shell excitation scheme described in the present paper, with the light source inside the shell, should thus allow for the measurement of much weaker coupling effects than the external scattering geometry previously used.

Figure 5a shows how the film thickness influences the resonances in the spectrum of transmitted light from a 477 nm bead. Both peaks shift toward blue with increasing Au film thickness, Figure 5b. We have used eq 1 to estimate the influence of the film thickness on the peak shift in the hybridization model framework. We found that the symmetric SPs have wavelengths and shifts similar to the experimental values, Figure 5c. Antisymmetric SPs would red shift with increasing film thickness, Figure 5d. Therefore, it is likely that the particular geometry of our system preferentially excites symmetric SP modes. However, some peaks, for example, the peak at 623 nm, for a 770 nm bead coated by 150 nm Au, seem much less sensitive than others to the metal film thickness. Such peaks are probably associated with a cavity mode rather than a surface mode and therefore less prone to influences occurring at the outer surface. However, a detailed description of the observed resonances has to take into account the fact that the bead sizes used in this experiment require multipolar contributions to be included. Moreover, the existence of the input aperture and the significant roughness of the film preclude the utilization of simple analytical treatments such as the Mie scattering theory for spherical objects. Instead, a numerical computational treatment is required; work in this direction is on its way in our group.

For sensing purposes, the most interesting resonances are those associated with surface modes, in other words, those peaks which are the most affected by the metal film thickness. Thus, we have found that, for the 770 nm spheres, the peak at ~720 nm is one of the most sensitive to the presence of adsorbates. It should be noted that some variation in the peak position will always occur due to variations in the film thickness and/or the size dispersion of the dielectric beads.

Figure 6a shows the spectral changes occurring upon admission of water and ethanol (3:1 v/v) vapors to the sensor. The sensor recovers completely after the saturated vapors are removed, Figure 6b, and can be cycled an indeterminate number of times without signs of saturation. The signals presented in Figure 6 cannot come from a change of the refractive index of the bulk air surrounding the bead. When the humidity changes from 50% (ambient) to ~100%, the change in the index of refraction of the ambient atmosphere is $\Delta n \approx 10^{-4}$, which is too small to result in the significant shift observed in Figure 6.[23] However, it has been shown that a several nanometers thick film of liquid water on a polycrystalline Au surface and possible condensation of fine droplets at the grain boundaries occur when the ambient humidity is increased.[24] In this case, spectral shifts on the order of several nanometers are expected, as suggested by previous experiments done with thin dielectric layers on other SPR nanosensors.[8,16,25,26]

To further verify that the spherical cavity sensor is indeed sensitive to surface modifications, we have employed alkanethiol adsorption from ethanol as a probe. The kinetics of adsorption of alkanethiols on gold films has been studied extensively.[27−30] Formation of a single monolayer is known to occur in ∼100 min at a ∼10 mM concentration. The spectra of the light scattered from the bead have been measured with the sample immersed in ethanol and after equilibration for several hours in a 10 mM solution of dodecanethiol in ethanol. A comparison of the spectra is provided in Figure 7a together with the spectral transmission of the flat gold film in the same conditions.

The spectral shifts in Figure 7a persist after the dodecanethiol solution is flushed with pure ethanol, indicating that irreversible adsorption of alkanethiol has occurred. The shifts are thus due to the formation of a monolayer at the gold surface.

Upon measurement of adsorption kinetics and fitting with a first-order exponential decay, we have found a time constant for the film formation of 382 ± 7 s at a 100 mM dodecanethiol concentration, which is somewhat slower than what has been previously measured on flat Au surfaces.[28] However, one should keep in mind that the Au film in our case is significantly rougher with respect to the evaporatively coated films which have been used in the previous reports. This fact may be at the origin of the discrepancy in the overall adsorption kinetics between previously reported data and our findings.

It is worth noting that, while the signal in Figure 7b corresponds to a single monolayer, the signal-to-noise ratio is good enough to provide sensitivities able to detect binding of fractions of a monolayer.

Conclusion

In conclusion, we have designed and implemented a resonant microcavity sensor made from a spherical gold-coated dielectric microparticle, which is excited through a near-field pinhole. The light scattered from the coated microparticle exhibits strong spectral resonances associated with the coupling of surface plasmon modes. These resonances can be used for sensing purposes, in a way similar to that of the surface plasmon resonances used for studies of molecular binding on planar surface plasmon sensors, but with the advantages of the submicrometer footprint and the high quality factors of microspherical resonators. The nature of these resonances is clearly related to shape, but their exact localization and excitation mechanisms need further investigation.

Acknowledgment. We are grateful to Dr. W. L. Schaich for many insightful comments. The donors of the Petroleum Research Fund, administered by the American Chemical Society, are acknowledged for partial support of this research. D.A. acknowledges Dr. J. A. Glazier for support from NSF Grant IBN-0083653, NASA Grant NAG 2-1619, a PTL fellowship, and an IBM Innovation Institute award, and support from the Biocomplexity Institute and the College of Arts and Sciences at Indiana University.

References and Notes

(1) Kielmann, F. *J. Microsc. (Oxford)* **1999**, *194*, 567.
(2) Yokota, H.; Saito, K.; Yanagida, T. *Phys. Rev. Lett.* **1998**, *80*, 4606.
(3) Ebbesen, T. W.; Lezec, H. J.; Ghaemi, H. F.; Thio, T.; Wolff, P. A. *Nature* **1998**, *391*, 667.
(4) Zawadzka, J.; Jaroszynski, D. A.; Carey, J. J.; Wynne, K. *Nucl. Instrum. Methods Phys. Res., Sect. A* **2000**, *445*, 324.
(5) Goodrich, T. T.; Lee, H. J.; Corn, R. M. *J. Am. Chem. Soc.* **2004**, *126*, 4086.
(6) Van Duyne, R. P. *Science* **2004**, *306*, 985.
(7) Jin, R. C.; Wu, G. S.; Li, Z.; Mirkin, C. A.; Schatz, G. C. *J. Am. Chem. Soc.* **2003**, *125*, 1643.
(8) Bohn, P. W. *Annu. Rev. Mater. Sci.* **1997**, *27*, 469.
(9) Bate, A. E. *Proc. Phys. Soc.* **1938**, *50*, 293.
(10) Collot, L.; Lefevreseguin, V.; Brune, M.; Raimond, J. M.; Haroche, S. *Europhys. Lett.* **1993**, *23*, 327.
(11) Vollmer, F.; Braun, D.; Libchaber, A.; Khoshsima, M.; Teraoka, I.; Arnold, S. *Appl. Phys. Lett.* **2002**, *80*, 4057.
(12) Vollmer, F.; Arnold, S.; Braun, D.; Teraoka, I.; Libchaber, A. *Biophys. J.* **2003**, *85*, 1974.
(13) Symes, R.; Sayer, R. M.; Reid, J. P. *Phys. Chem. Chem. Phys.* **2004**, *6*, 474.
(14) Kwak, E. S.; Onuta, T. D.; Amarie, D.; Potyrailo, R.; Stein, B.; Jacobson, S. C.; Schaich, W. L.; Dragnea, B. *J. Phys. Chem. B* **2004**, *108*, 13607.
(15) Schug, C.; Lamparter, P.; Steeb, S. *Surf. Interface Anal.* **1999**, *27*, 670.
(16) Raether, H. *Surface Plasmons on Smooth and Rough Surfaces and on Gratings*; Springer-Verlag: Berlin, 1985.
(17) Aden, A. L.; Kerker, M. *J. Appl. Phys.* **1951**, *22*, 1242.
(18) Prodan, E.; Radloff, C.; Halas, N. J.; Nordlander, P. *Science* **2003**, *302*, 419.
(19) Jackson, J. B.; Halas, N. J. *Proc. Natl. Acad. Sci. U.S.A.* **2004**, *101*, 17930.
(20) Prodan, E.; Lee, A.; Nordlander, P. *Chem. Phys. Lett.* **2002**, *360*, 325.
(21) Coyle, S.; Netti, M. C.; Baumberg, J. J.; Ghanem, M. A.; Birkin, P. R.; Bartlett, P. N.; Whittaker, D. M. *Phys. Rev. Lett.* **2001**, *8717*, art. no.
(22) West, J. L.; Halas, N. J. *Annu. Rev. Biomed. Eng.* **2003**, *5*, 285.
(23) *CRC Handbook of Chemistry and Physics*; Lide, D. R., Ed.; CRC Press: New York, 2003.
(24) Gil, A.; Colchero, J.; Gomez-Herrero, J.; Baro, A. M. *Ultramicroscopy* **2001**, *86*, 1.
(25) Templeton, A. C.; Pietron, J. J.; Murray, R. W.; Mulvaney, P. *J. Phys. Chem. B* **2000**, *104*, 564.
(26) Jensen, T. R.; Duval, M. L.; Kelly, K. L.; Lazarides, A. A.; Schatz, G. C.; Van Duyne, R. P. *J. Phys. Chem. B* **1999**, *103*, 9846.
(27) Pan, W.; Durning, C. J.; Turro, N. J. *Langmuir* **1996**, *12*, 4469.
(28) Damos, F. S.; Luz, R. C. S.; Kubota, L. T. *Langmuir* **2005**, *21*, 602.
(29) Shimazu, K.; Yagi, I.; Sato, Y.; Uosaki, K. *Langmuir* **1992**, *8*, 1385.
(30) Bain, C. D.; Troughton, E. B.; Tao, Y. T.; Evall, J.; Whitesides, G. M.; Nuzzo, R. G. *J. Am. Chem. Soc.* **1989**, *111*, 321.